Catalysis Science & Technology

www.rsc.org/catalysis

Volume 3 | Number 10 | October 2013 | Pages 2447–2850

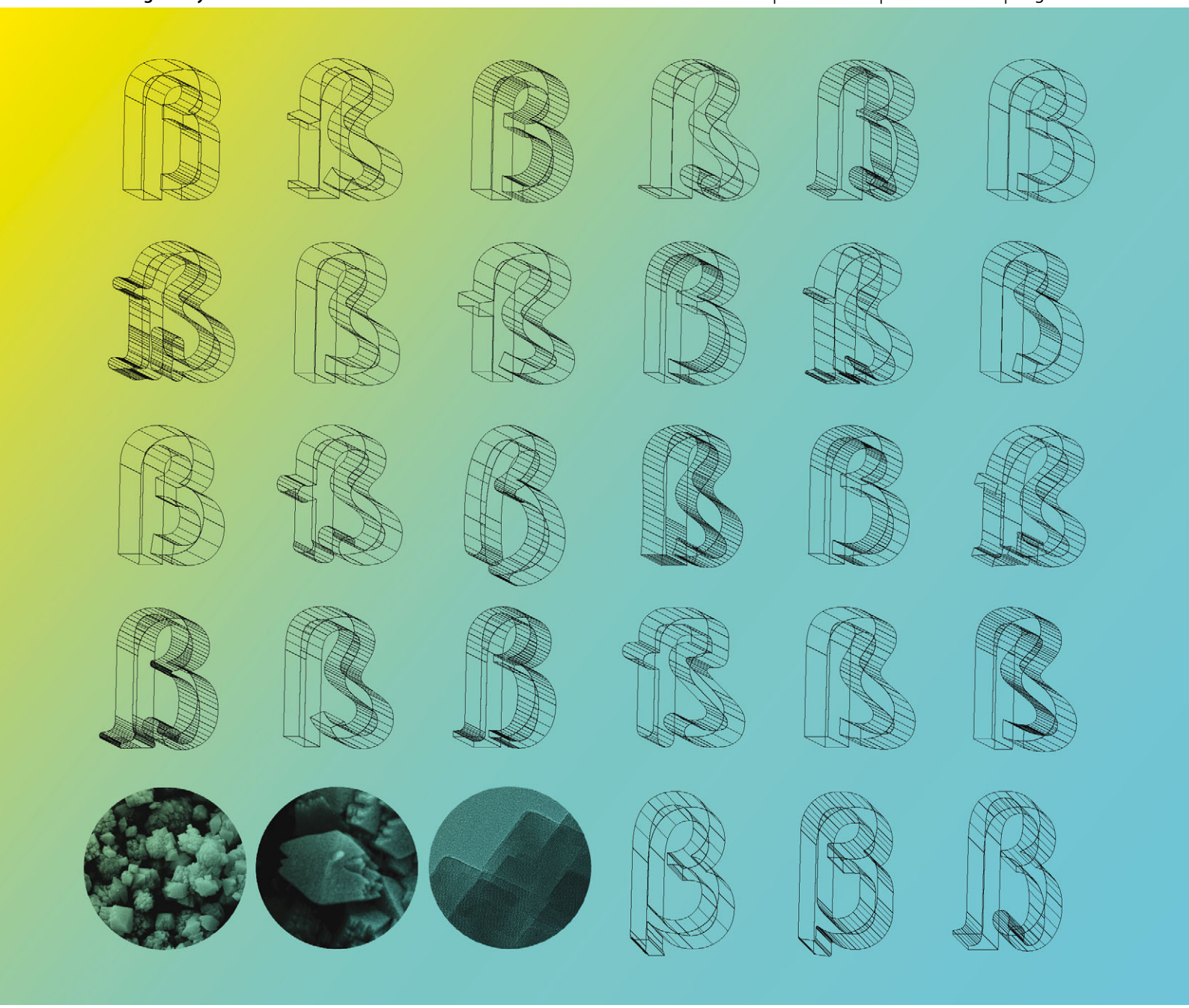

ISSN 2044-4753

RSC Publishing

COVER ARTICLE

Yilmaz *et al.*

A new catalyst platform: zeolite Beta from template-free synthesis

Catalysis
Science & Technology

RSC Publishing

PAPER

View Article Online
View Journal | View Issue

Cite this: Catal. Sci. Technol., 2013, 3, 2580

A new catalyst platform: zeolite Beta from template-free synthesis†

Bilge Yilmaz,*[a] Ulrich Müller,[b] Mathias Feyen,[b] Stefan Maurer,[b] Haiyan Zhang,[c] Xiangju Meng,[d] Feng-Shou Xiao,[d] Xinhe Bao,[e] Weiping Zhang,[f] Hiroyuki Imai,[g] Toshiyuki Yokoi,[h] Takashi Tatsumi,[h] Hermann Gies,[i] Trees De Baerdemaeker[j] and Dirk De Vos[j]

Received 8th December 2012,
Accepted 30th April 2013

DOI: 10.1039/c3cy00073g

www.rsc.org/catalysis

Structural analysis and catalytic testing revealed that zeolite Beta from template-free synthesis introduces new possibilities in catalysis, as a result of its unprecedentedly high density of active sites with exceptional stability and distinctively ordered nature. Highly active and selective catalysts were obtained either by using it in the Al-rich form (*e.g.* alkylation) or after post-synthesis treatments (*e.g.* acylation). Such versatility made possible by this novel synthesis route constitutes a new toolbox for catalysis.

Introduction

As a well-established family of nanoporous catalysts, zeolites are of vital importance for the chemical and petrochemical industries. Zeolite Beta, with its intriguing framework architecture (*BEA) and 3-dimensional pore system, displays superior performance in refinery applications, environmental catalysis and a variety of organic reactions because of its vastly accessible pore volume, high adsorption capacity, strong acid sites and shape/size selectivity.[1] Zeolite Beta for industrial utilization is typically synthesized using tetraethylammonium hydroxide (TEAOH) as the template or structure directing agent (SDA).[2] Various higher cost organic templates were also explored.[3] Recently, Xiao and co-workers reported a template-free (TF) synthesis methodology for zeolite Beta,[4] which was later shown to be applicable to some other zeolite types as well.[5] Subsequently, SDA-free synthesis of zeolite Beta was also explored by Okubo, Mintova and their teams.[6] Related to these efforts, another interesting field of study is the solvent-free synthesis of zeolites, where there have been recent reports on a number of structures including zeolite Beta.[7]

A vast majority of the synthetic zeolites that offer promise as industrial catalysts require organic SDAs for their synthesis. If they end up being commercialized, they are classified as "specialty" zeolites from an industrial point of view, which translates into a prohibitive cost structure for many applications. For industrial production, SDA-free synthesis means significant savings in raw material, energy and capital investment. It completely avoids the energy-intensive high temperature calcination, thereby eliminating the formation of harmful combustion gases. In addition, the SDA-free route allows the utilization of simpler low-pressure vessels, with significant cost savings. Therefore, even zeolites previously considered to be too expensive can now be employed in petrochemical applications.

Moreover, the SDA-free synthesis has a major influence on the product characteristics. Preliminary analyses demonstrated that Beta zeolites from SDA-free synthesis exhibit a significantly larger crystal size and an unprecedentedly high aluminum content compared to the conventional templated zeolite Beta.[5,6] Here, we report detailed structural investigations and catalytic tests using SDA-free Beta, not only in the as-synthesized form but also after controlled modifications. As will be demonstrated, the SDA-free Beta as such has striking activity and selectivity characteristics, because of its significantly higher density of active sites and uniquely ordered nature. Additionally, the material can be

[a] BASF Corporation, Iselin, NJ 08830, USA. E-mail: bilge.yilmaz@basf.com
[b] BASF SE, Ludwigshafen, Germany
[c] College of Chemistry, Jilin University, Changchun, China
[d] Department of Chemistry, Zhejiang University, Hangzhou, China
[e] State Key Laboratory of Catalysis, Dalian Institute of Chemical Physics, Dalian, China
[f] State Key Laboratory of Fine Chemicals, Dalian University of Technology, Dalian, China
[g] Department of Chemical and Environmental Engineering, University of Kitakyushu, Fukuoka, Japan
[h] Chemical Resources Laboratory, Tokyo Institute of Technology, Yokohama, Japan
[i] Institute of Geology, Mineralogy and Geophysics, Ruhr-University Bochum, Bochum, Germany
[j] Centre for Surface Chemistry and Catalysis, K. U. Leuven, Heverlee, Belgium

† Electronic supplementary information (ESI) available: Additional structural, characterization and catalytic testing data. See DOI: 10.1039/c3cy00073g

modified in a controlled way to emulate the properties of the more expensive templated Beta with a higher Si/Al ratio. Even though templated and SDA-free Beta share the *BEA framework, their growth mechanisms, physicochemical characteristics and resulting structure–property relationships are markedly diverse. In this contribution, the superior catalytic performance of SDA-free Beta, in the as-synthesized and modified forms, is demonstrated in alkylations and acylations.

Experimental

SDA-free synthesis of zeolite Beta

The zeolitic products with the *BEA framework were synthesized starting from aluminosilicate synthesis mixtures at temperatures between 120–140 °C in the presence of previously calcined zeolite Beta seeds. A wide variety of zeolite Beta materials were explored as seeds and it was shown that zeolite Beta with varying characteristics can be utilized for this purpose. In this contribution, characterization and catalytic testing of the products from SDA-free syntheses utilizing the calcined CP814C zeolite Beta (Zeolyst) seeds are reported. The powder XRD pattern for the seed crystals used in this investigation is provided in Fig. S1 (ESI†). The role of seed crystals in SDA-free synthesis has been discussed in detail elsewhere.[5,6] Fumed silica, sodium aluminate (Al_2O_3 > 41.0%), and sodium hydroxide (NaOH > 96%) were used as the ingredients for the synthesis mixture. In a typical synthesis experiment the following recipe was used:

(1) 0.07 g $NaAlO_2$ was dissolved in 7.56 mL distilled water, followed by addition of 0.312 g of NaOH;

(2) After stirring for 30 minutes, 0.72 g of fumed silica was added to the solution obtained in step (1);

(3) After stirring for 10 minutes, 0.036 g of zeolite Beta seeds were introduced into the synthesis mixture, followed by stirring for 3 minutes;

(4) The resulting gel with a molar ratio of $SiO_2 : 0.025Al_2O_3 : 0.36Na_2O : 35{\cdot}3H_2O$ was transferred into a 15 mL Teflon-lined stainless-steel autoclave to crystallize at 120 °C for 120 hours in an oven;

(5) After filtration at room temperature and drying at 80 °C, solid products were recovered.

To convert the as-synthesized samples from the Na^+-form to the H^+-form, they were subjected three times to an ion-exchange treatment with 0.5 M NH_4NO_3 at 80 °C overnight followed by washing with distilled water, drying and heat treatment at 450 °C for 5 hours (heating rate 1 °C min^{-1}).

Steam-dealumination of the as-synthesized samples was performed after ion-exchange with NH_4NO_3 followed by repeated steam treatment. Before each steam treatment the sample was treated with an aqueous NH_4NO_3 solution at reflux followed by washing and drying. For the steam treatment, the sample was hydrated and heated in a covered vessel to 600 °C for 2 hours.

After steam treatment, part of the dealuminated sample was further treated with acid using a 1 M HNO_3 solution at 80 °C for 3 hours followed by washing and drying at 80 °C. Another part of the dealuminated sample was ion-exchanged three times with a 4 M NH_4NO_3 solution at 100 °C for 2 hours followed by ammonia removal *via* heat treatment.

Commercial zeolite CP811 was obtained in the H^+-form from Zeolyst. Commercial zeolite CP814C ($NH4^+$-form, Zeolyst) was converted to the H^+-form by calcination at 450 °C for 5 hours.

Characterization

High-resolution X-ray powder diffraction data for samples to be compared were collected at room temperature with a Siemens D5000 diffractometer operating in quasi Debye–Scherrer mode using both Mo-Kα and Cu-Kα radiation with the sample in a capillary sample holder. ^{29}Si MAS NMR spectra were recorded at 79.5 MHz with ^{1}H decoupling at a spinning rate of 6 kHz, 1000 scans, and 4 s recycle delay. The chemical shifts were referenced to tetramethylsilane. ^{27}Al 3Q MAS NMR experiments were performed on a Varian Infinityplus-400 spectrometer using a three-pulse sequence incorporating a Z-filter at a spinning speed of 12 Hz with a 4 mm probe. The spectra were acquired at 104.2 MHz, and the chemical shifts were referenced to a 1.0 wt% $Al(NO_3)_3$ aqueous solution. An rf field of 227 kHz was used for the creation (0 Q → 3 Q) and the first conversion (+3 Q → 0 Q) pulse. An rf field of 17 kHz was used for the last conversion step (0 Q → ±1 Q), which was the central transition selective soft 90° pulse. A two-dimensional (2D) Fourier transformation followed by a shearing transformation gave a pure absorption mode 2D contour plot. The second order quadrupolar effect (SOQE) and isotropic chemical shift (δ_{iso}) values were calculated according to the procedures in literature.

Temperature programmed desorption of ammonia (NH_3-TPD) experiments were performed using an automated chemisorption analysis unit with a thermal conductivity detector (TCD). This setup was also equipped with an on-line mass spectroscopy (MS) system for continuous analysis of the desorbed species.

Infrared spectra of self-supporting wafers of the Beta zeolite samples (H^+-form) with a thickness of 10–20 mg cm^{-2} were measured on a Nicolet 6700 FT-IR spectrometer. Spectra were taken at 150 °C after heating under vacuum to 450 °C (heating rate 5 °C min^{-1}) and evacuating for 1 hour.

Bulk elemental analysis of the samples was performed using a Varian Vista-PRO inductively coupled plasma optical emission spectrometer (ICP-OES). Field emission scanning electron microscopy (FE-SEM) was performed using a JEOL JSM-7400F unit to determine the crystal size.

Catalytic reactions

Alkylation of benzene with ethylene was performed in a Parr autoclave with a capacity of 100 mL, loaded under nitrogen with 40 mL benzene (99.7%, Sigma-Aldrich) and 62.5 mg catalyst, which had been dried overnight in an oven at 150 °C. The reactor was flushed and saturated with ethylene (99.95%, Air Liquide) at a pressure of 5 bar for 30 minutes and pressurized with 50 bar nitrogen and heated to 150 °C. The stirring speed was set at 1000 rpm. Samples were taken periodically and analyzed on a Shimadzu 2010 GC equipped with a CP-Sil-5CB 60 m column and an FID detector and by GC/MS. The ethylbenzene or diethylbenzene

selectivity was determined by calculating the molar ratio of ethylbenzene or diethylbenzene to the sum of all reaction products derived from ethylene.

Acylation of anisole with acetic anhydride was performed in a round-bottom flask with a capacity of 10 mL. 50 mg of the catalyst, which was dried overnight in an oven at 100 °C, was added to a mixture of 50 mmol anisole (99%, Acros Organics) and 5 mmol acetic anhydride (98%, VWR) in the flask. The flask containing the catalyst and the reactants was sealed, and then heated in an oil bath at 60 °C for 5 hours under stirring with a magnetic stirrer. Analysis of the reaction products was performed using a Shimadzu 2014GC equipped with a DB-5 50 m column and an FID detector.

Results and discussion

Morphological analysis of zeolite Beta products from SDA-free synthesis shows significantly larger crystal size in the 200–700 nm range, and correspondingly more prominent textural features compared to the templated zeolite Beta, which typically displays particle sizes between 20 and 100 nm.[5] SDA-free synthesis also influences the overall porosity of zeolite Beta: the as-synthesized product has significantly higher micropore surface area and larger median pore size with respect to the templated zeolite Beta after calcination. The considerably lower Si/Al ratio (4.5–5) and the higher (hydro)thermal stability of zeolite Beta from SDA-free synthesis are other notable deviations from templated zeolite Beta.[4,5] The underlying reasons for these apparent differences for zeolitic materials with the same framework topology must be traced back to structural differences as a result of their distinct formation mechanisms and building blocks. In order to develop an understanding of this phenomenon, and to potentially use these findings to tailor-make catalysts for specific reactions, we have first undertaken a targeted structural investigation of the products from SDA-free synthesis.

Analysis of the powder XRD-pattern of zeolite Beta from SDA-free synthesis (TF-Beta) reveals two significant features (Fig. 1). It is immediately obvious that the stacking disorder of the layered building block is very similar to that of the mineral Tschernichite and also to that of templated zeolite Beta.[8] Simulations of the stacking disorder using DIFFaX show that the simulated powder XRD-pattern gave the best fit with an intergrowth of 44% of the A-polymorph and 56% of the B-polymorph. Therefore, TF-Beta benefits from the interconnected 12MR system of the silicate skeleton, without the structural features the ordered end-members would have (Fig. S2, ESI†). Inspecting the powder XRD-pattern more closely and focusing on those reflections which are not broadened by the structural disorder, *e.g.* (008) at ~12.3° 2θ Mo-Kα radiation (Fig. S3, ESI†), it is obvious that the inherent linewidth is much smaller than for the templated zeolite Beta material. In Fig. S3 (ESI†), the full width at half maximum (FWHM) of (008) of TF-Beta was determined to be 0.061° 2θ as compared to 0.083° 2θ for templated zeolite Beta, a CP814 material from Zeolyst. This implies that the material from SDA-free synthesis possesses fewer structural defects, yielding a significantly improved crystallinity. The higher degree of order for TF-Beta might also explain the unusually high hydrothermal stability of this material as previously observed.[5] Typically, zeolites with such high aluminum content are much less stable compared to the high-silica zeolites.

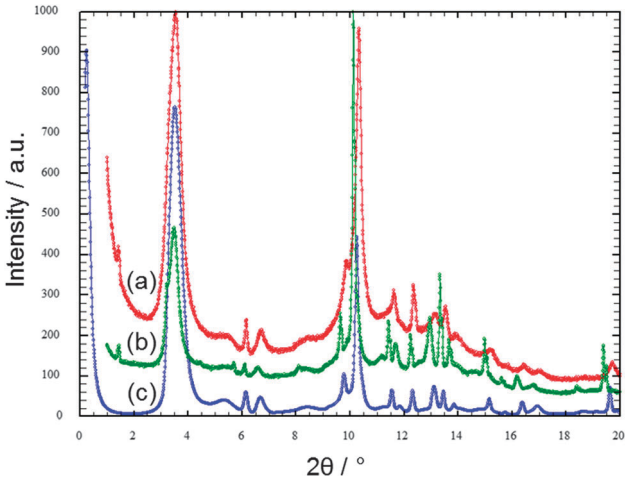

Fig. 1 XRD patterns (Mo-Kα radiation) for zeolite Beta from templated synthesis (a, CP814), SDA-free synthesis (b) and a simulation assuming 44% polymorph A content (c).

In order to confirm the higher degree of structural order in TF-Beta, quantitative ^{29}Si MAS NMR measurements were also performed and the results for products from conventional and SDA-free syntheses were compared. After deconvolution and integration of the spectra (Fig. 2), the full width at half maximum (FWHM) in Hz of various Si environments and the Si/Al ratios in the samples were obtained. The results are listed in Table S1 in the ESI.† As illustrated in Fig. 2 and Table S1 (ESI†), the FWHM of each of the Si species as determined from ^{29}Si MAS NMR spectra is narrower on TF-Beta than on conventional templated zeolite Beta. This finding confirms the more ordered nature of the TF-Beta zeolite.

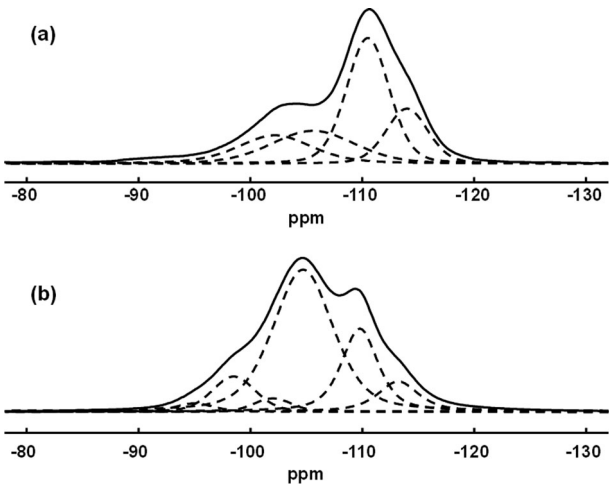

Fig. 2 ^{29}Si MAS NMR spectra with the deconvoluted peaks for zeolite Beta from templated synthesis (a, CP814, H^+-form) and SDA-free synthesis (b, H^+-form).

The extraordinarily high aluminum content of TF-Beta is definitely one of the most striking features of this material. It is the key characteristic in defining the catalytic performance, ion-exchange capacity and framework polarity of this zeolite. In addition, the potential for further functionalization *via* isomorphous substitution may also depend on the framework aluminum atoms. Therefore, understanding the nature of aluminum in TF-Beta and comparison to the templated system are of critical importance.

Two-dimensional ^{27}Al 3Q MAS NMR spectra were used to remove the anisotropic line broadening, allowing identification of species with similar isotropic chemical shifts but different quadrupolar coupling constants. As shown in Fig. 3a for the templated Beta (CP814, Si/Al = 19, H^+-form), the overlapping peaks observed in the ^{27}Al MAS spectrum at 54 ppm are clearly resolved in the F_2 field of the 3Q MAS NMR spectrum. These are assigned to tetrahedrally coordinated aluminum at different T-sites. Meanwhile, in the F_1 field two distinct framework aluminum species, designated as Al(IV)$_a$ and Al(IV)$_b$ with SOQE of 1.9 and 1.7 MHz, respectively, can be seen in the tetrahedral region. A third one, Al(VI)$_a$, is also observed in the octahedral environment at *ca.* 0 ppm with SOQE of 0.75 MHz. By contrast, for the aluminum rich TF-Beta (Si/Al = 4.6), after ammonium exchange and decomposition of NH_4^+ to protons (H^+-form, Fig. 3b), there is only one framework aluminum signal with SOQE of 2.3 MHz in the projection of the isotropical-chemical-shift field (F_1 field) with only very minor formation of 6-coordinated aluminum in non-lattice positions. This means that this large amount of aluminum occupies only a restricted number of T-sites. The high Al content will affect the overall strain and the geometries in the structure; therefore, the different Al-sites in the H-form of TF-Beta cannot be further resolved or assigned.

In order to confirm the structural differences observed above between TF-Beta and conventional templated zeolite Beta, another commercial zeolite Beta sample (CP811, H^+-form) was also investigated following the same procedure. Two-dimensional ^{27}Al 3Q MAS NMR spectrum for this commercial zeolite Beta sample with slightly higher Al content (Si/Al = 12) is presented in Fig. S4 (ESI†). For this sample, in the F_1 field two distinct framework aluminum species, designated as Al(IV)$_a$ and Al(IV)$_b$ with SOQE of 1.7 and 1.6 MHz, respectively, can be detected in the tetrahedral region. A third one, Al(VI), is also observed in the octahedral environment at *ca.* 0 ppm with SOQE of 1.2 MHz. These findings provide another comparison with the conventional zeolite Beta products from templated syntheses and confirm the distinct nature of the Al-sites in TF-Beta.

The acidity of TF-Beta was investigated using NH_3 temperature-programmed desorption. Fig. 4 shows the NH_3-TPD profiles of two templated Beta zeolites (CP811 with Si/Al of 12 and CP814 with Si/Al of 19) and TF-Beta. NH_3-TPD profiles are also given for these samples after steam-dealumination and further NH_4^+ ion-exchange or acid treatment. All Beta zeolites show two peaks in the TPD profile. TF-Beta shows a much larger amount of desorbed NH_3 than the templated Beta zeolite, in agreement with its larger aluminum content and number of acid sites. Remarkably, the strength of the strongest acid sites, as evaluated

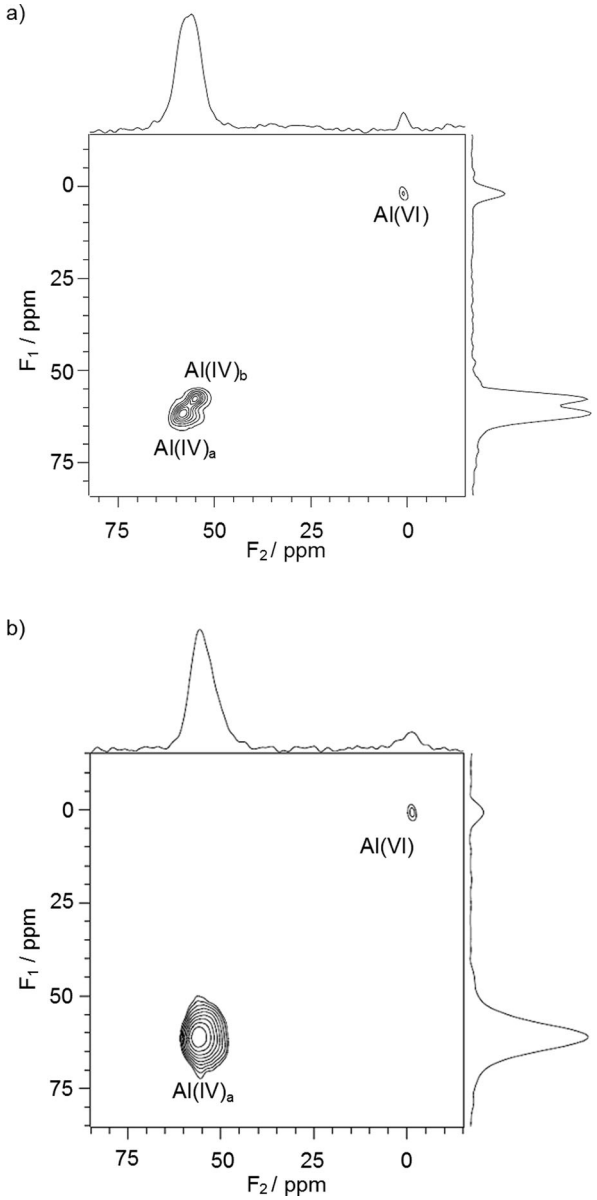

Fig. 3 Two-dimensional ^{27}Al 3Q MAS NMR spectra of templated zeolite Beta (a, CP814, H^+-form) and TF-Beta (b, H^+-form). The corresponding ^{27}Al MAS NMR spectrum is given on the top of the 3Q MAS plot. The F_1 projection is the pure isotropic spectrum.

from the maximum of the second NH_3 desorption peak, is the same for as-prepared TF-Beta as for the templated Beta. After steam-dealumination, the amount of desorbed NH_3 decreases and after subsequent acid treatment, the first desorption peak becomes smaller than the second. This indicates that controlled modification allows us to vary the number of the acid sites over a broad range, while keeping the strength of the strongest acid sites at least at the same high level. The sharper TPD peaks for TF-Beta derived samples in comparison with the templated material are in excellent agreement with more uniform and well-defined acid sites. ^{27}Al MAS NMR spectrum of the steam-dealuminated TF-Beta (Fig. S5, ESI†) exhibited a broad peak at around 30 ppm together with peaks attributed to tetrahedrally

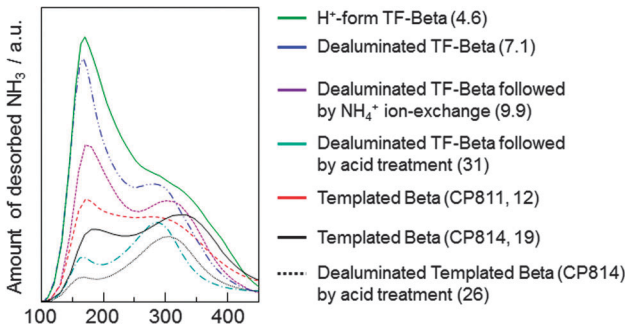

Fig. 4 NH_3-TPD profiles of Beta zeolites (Si/Al ratios between brackets).

and octahedrally coordinated Al species. The broad peak at around 30 ppm was no longer observed on the samples that were obtained by treating the steam-dealuminated zeolite with either HNO_3 aq. or NH_4NO_3 aq. (Fig. S5, ESI†). Moreover, octahedrally coordinated Al species were also removed by acid treatment of the steam-dealuminated TF-Beta, leaving aluminum only in tetrahedral framework positions.

Fig. 5 shows the O–H stretching vibration domains in the IR spectra of protonic forms of a templated Beta zeolite (CP811) and of TF-Beta. For CP811 the hydroxyl vibrations at 3742 cm^{-1} and 3735 cm^{-1} are dominant. These correspond to the non-acidic silanol groups at the outer surface of the zeolite crystals and at structural defects inside the crystals, respectively.[9] TF-Beta has a much lower concentration of such hydroxyl groups, in agreement with its significantly higher degree of crystalline order and larger crystal size. For TF-Beta the bridging hydroxyl groups at 3607 cm^{-1} are much more prominent compared to the other Beta zeolites, in line with the high concentration of well-defined Brønsted acidic sites. A vibration of minor intensity is observed for TF-Beta at 3660 cm^{-1}, corresponding to hydroxylated monomeric or polymeric extra-framework aluminum species, which is in line with the NMR characteristics of the TF-Beta after conversion to the H^+-form (Fig. 3b).

The distinct structural features of TF-Beta also translate into unique catalytic properties for this material. The alkylation of benzene with ethylene and the acylation of anisole with acetic anhydride were selected here as model cases for respectively TF-Beta as such, or TF-Beta after controlled modification. In Fig. 6 the benzene conversion in the alkylation of benzene with ethylene at 150 °C is given for the commercial Beta zeolites CP811 (Si/Al = 12) and CP814 (Si/Al = 19) and for TF-Beta (Si/Al = 4.6), at a benzene : ethylene ratio of 8. Full ethylene conversion is reached for all catalysts after 24 hours. TF-Beta shows a higher initial activity than the commercial catalysts in this alkylation reaction. This shows that in spite of its high aluminum content, the acid sites of TF-Beta are of sufficient strength and number to catalyze this demanding ethylation reaction. At all measured conversions, the selectivity to ethylbenzene (Fig. 6) is distinctly higher for TF-Beta than for the various templated Beta zeolites. At increasing conversions, this is accompanied by a lower selectivity to diethylbenzene (Fig. S6, ESI†). This higher selectivity towards the monoalkylated

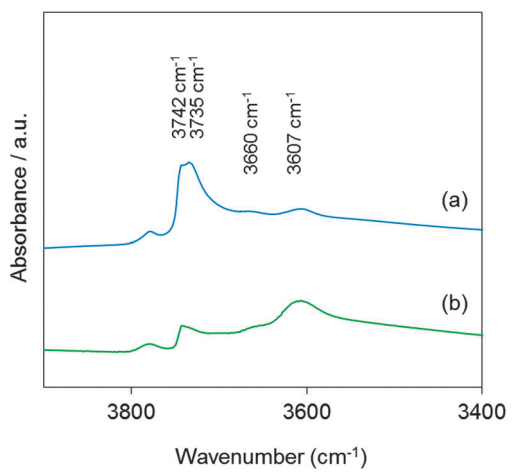

Fig. 5 Infrared spectra of template zeolite Beta (a, CP811) and TF-Beta (b) at 150 °C.

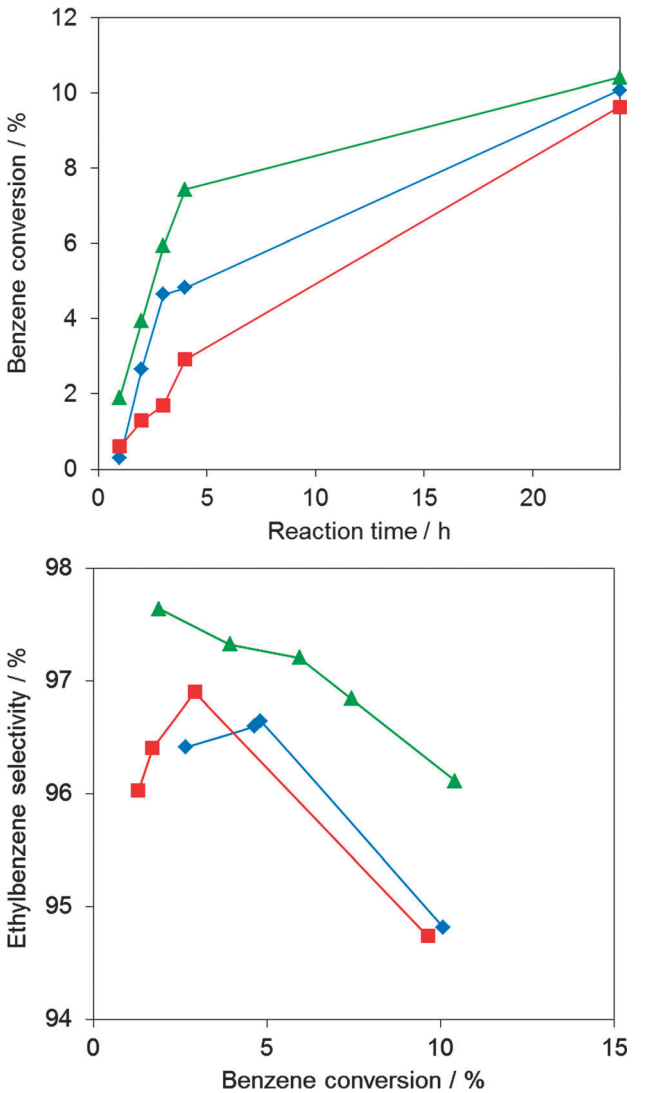

Fig. 6 Benzene ethylation (150 °C): (top) conversion *vs.* time (hours), and (bottom) selectivity *vs.* conversion for templated Beta zeolites CP814 (■) and CP811 (◆), and for TF-Beta (▲).

Table 1 Catalytic activity of zeolite Beta materials originating from TF-Beta in comparison to those originating from templated Beta for the acylation of anisole with acetic anhydride[a]

Sample	Si/Al[b]	TON[c]	*p*-MAP yield[d] (%)
TF-Beta	4.6	—	0
Steam-dealuminated TF-Beta	7.1	11	38
Acid-treated dealuminated TF-Beta	31	54	48
NH_4^+ exch., dealuminated TF-Beta	9.9	15	54
CP811	12	26	22
CP814	19	30	38
Acid-treated CP814	26	35	36

[a] Reaction conditions: 60 °C, 50 mg catalyst in H^+ form, 50 mmol anisole, 5 mmol acetic anhydride. [b] Measured by ICP. [c] TON in mol (mol Al)$^{-1}$. [d] After 5 hours of reaction.

product is readily explained by the higher framework polarity of the aluminum-rich TF-Beta, which favors adsorption of benzene over that of ethylbenzene and therefore facilitates the ethylbenzene desorption.

As a second reaction to demonstrate the potential of catalysts derived from TF-Beta, the Friedel–Crafts acylation of anisole with acetic anhydride was performed on TF-Beta and on commercial Beta zeolites CP811 and CP814. Results are summarized in Table 1. The H^+-form of TF-Beta (Si/Al = 4.6) showed no activity for the acylation of anisole even after 24 h. However, other Beta samples derived from TF-Beta through various post-synthesis treatments were highly productive for *p*-methoxyacetophenone (*p*-MAP, selectivity > 99%). *p*-MAP yields based on the initial amount of acetic anhydride are compared in Table 1. While dealumination of TF-Beta by steam treatment decreased the aluminum content (Si/Al = 7.1), the catalytic activity was dramatically improved and this steam-dealuminated TF-Beta showed a much higher conversion (*p*-MAP yield = 38%) than the templated zeolite Beta with the lowest Si/Al ratio (Si/Al = 12, *p*-MAP yield = 22%) after 5 hours of reaction. Acid treatment of the steam-dealuminated TF-Beta further enhanced the catalytic activity (48% conversion after 5 hours), although the aluminum content of the zeolite was noticeably decreased (Si/Al = 31). Meanwhile, NH_4^+ ion-exchange treatment of the steam-dealuminated TF-Beta followed by calcination (Si/Al = 9.9) led to an even higher catalytic activity (54% at 5 hours). The turnover number (TON) at 30 minutes for each catalyst was estimated based on the aluminum content in the catalyst and the amount of consumed acetic anhydride. Acid-treated dealuminated TF-Beta showed a remarkably high TON of 54 in comparison to the templated zeolite Beta samples with Si/Al of 12 (TON = 26) and 19 (TON = 30). For comparison of this highly active TF-Beta sample (Si/Al = 31) with the templated zeolite Beta at a similar Si/Al ratio, the commercial zeolite Beta sample with the higher Al content (CP814) was also subjected to the acid treatment. The resulting catalyst had a comparable Si/Al ratio (Si/Al = 26), yet the *p*-MAP yield was significantly lower (*p*-MAP yield = 36%) compared to the acid-treated dealuminated TF-Beta.

The low activity of the aluminum-rich TF-Beta in this reaction can be explained by its high framework polarity. This renders the desorption of the more polar *p*-MAP more difficult, leading to fast catalyst deactivation. On the one hand, dealumination of TF-Beta leads to a less polar material that is more resistant to deactivation which explains the higher activity of the dealuminated TF-Beta samples. On the other hand, dealumination also decreases the number of acid sites, as can be seen from the NH_3-TPD profiles (Fig. 4). This explains why even though the acid-treated dealuminated TF-Beta has the highest TON, its overall *p*-MAP yield is lower than that of the Al-richer NH_4^+ ion-exchanged dealuminated TF-Beta, the latter showing the best combination of acid site strength, concentration and framework polarity.

Conclusions

In summary, SDA-free synthesis of zeolite Beta is not only economically attractive, but also results in zeolitic products with superior catalytic performance. The as-synthesized material possesses a high density of active sites with exceptional stability and distinctively ordered nature, useful in *e.g.* ethylation of benzene; after dealumination and/or other post-synthesis treatments, catalysts with varying Si/Al ratios, suitable *e.g.* for acylation of anisole, are obtained. The ability to manipulate the framework aluminum content in a very broad range, while maintaining structural integrity, proves that TF-Beta zeolites constitute a powerful toolbox for designing new acid catalysts.

This work was performed under the framework of the INCOE (International Network of Centers of Excellence) project coordinated by BASF. T.D.B. acknowledges F.W.O.-Vlaanderen (Research Foundation – Flanders) for a doctoral fellowship. The authors thank Prof. A. Atıf Akın of Rutgers University for his help with the cover page artwork.

Notes and references

1 (*a*) G. Bellussi, G. Pazzuconi, C. Perego, G. Girotti and G. Terzoni, *J. Catal.*, 1995, **157**, 227–234; (*b*) R. A. Innes, S. I. Zones and G. J. Nacamuli, *US 4891458*, Chevron Research Company, 1990; (*c*) M. Spagnol, L. Gilbert, E. Benazzi and C. Marcilly, *US 5817878*, Rhone-Poulenc Chimie, 1998; (*d*) A. Corma, L. T. Nemeth, M. Renz and S. Valencia, *Nature*, 2001, **412**, 423–425; (*e*) T. F. Degnan and P. J. Angevine, *US 6652735*, ExxonMobil Research and Engineering Company, 2003; (*f*) L. Wang, *US 7169291*, UOP LLC, 2007; (*g*) H. Ohtsuka, T. Tabata, O. Okada, L. M. F. Sabatino and G. Bellussi, *Catal. Lett.*, 1997, **44**, 265–270; (*h*) B. Coq, M. Mauvezin, G. Delahay, J. B. Butet and S. Kieger, *Appl. Catal., B*, 2000, **27**, 193–198.

2 R. L. Wadlinger, G. T. Kerr and E. J. Rosinski, *US 3308069*, 1967.

3 (*a*) J. C. van der Waal, M. S. Rigutto and H. van Bekkum, *J. Chem. Soc., Chem. Commun.*, 1994, 1241–1242; (*b*) P. Caullet, J. Hazm, J. Guth, J. Joly, J. Lynch and F. Raatz, *Zeolites*, 1992, **12**, 240–250; (*c*) M. K. Rubin, *EP 0159847*, Mobil Oil Corporation, 1989; (*d*) J. Van der Waal, P. Kooyman, J. Jansen and H. Van Bekkum, *Microporous Mesoporous Mater.*, 1998, **25**, 43–57; (*e*) S. Zones,

Y. Nakagawa, L. T. Yuen and T. Harris, *J. Am. Chem. Soc.*, 1996, **118**, 7558–7567; (*f*) M. A. Camblor, L. A. Villaescusa and M. J. Díaz-Cabañas, *Top. Catal.*, 1999, **9**, 59–76.

4 B. Xie, J. Song, L. Ren, Y. Ji, J. Li and F. S. Xiao, *Chem. Mater.*, 2008, **20**, 4533–4535.

5 B. Xie, H. Zhang, C. Yang, S. Liu, L. Ren, L. Zhang, X. Meng, B. Yilmaz, U. Muller and F.-S. Xiao, *Chem. Commun.*, 2011, **47**, 3945–1947.

6 (*a*) Y. Kamimura, W. Chaikittisilp, K. Itabashi, A. Shimojima and T. Okubo, *Chem.–Asian J.*, 2010, **5**, 2182–2191; (*b*) Y. Kamimura, S. Tanahashi, K. Itabashi, A. Sugawara, T. Wakihara, A. Shimojima and T. Okubo, *J. Phys. Chem. C*, 2011, **115**, 744–750; (*c*) G. Majano, L. Delmotte, V. Valtchev and S. Mintova, *Chem. Mater.*, 2009, **21**, 4184–4191.

7 (*a*) R. E. Morris and S. L. James, *Angew. Chem., Int. Ed.*, 2013, **52**, 2163–2165; (*b*) L. Ren, Q. Wu, C. Yang, L. Zhu, C. Li, P. Zhang, H. Zhang, X. Meng and F.-S. Xiao, *J. Am. Chem. Soc.*, 2012, **134**, 15173.

8 R. Szostak, K. P. Lillerud and M. Stocker, *J. Catal.*, 1994, **148**, 91–99.

9 (*a*) A. Simon-Masseron, J. Marques, J. Lopes, F. R. Ribeiro, I. Gener and M. Guisnet, *Appl. Catal., A*, 2007, **316**, 75–82; (*b*) I. Kiricsi, C. Flego, G. Pazzuconi, W. O. J. Parker, R. Millini, C. Perego and G. Bellussi, *J. Phys. Chem.*, 1994, **98**, 4627–4634.

